JOURNAL OF SPACECRAFT AND ROCKETS
Vol. 33, No. 3, May–June 1996

Hypersonic Nozzle–Afterbody Experiment: Flowfield Surveys

Frank W. Spaid*
McDonnell Douglas Corporation, St. Louis, Missouri 63166
and
Earl R. Keener†
Eloret Institute, Palo Alto, California 94303

This study was conducted to characterize experimentally the flowfield created by the interaction of a single-expansion-ramp nozzle flow with a hypersonic external stream. Data were obtained from a generic nozzle–afterbody model in the 3.5-Ft Hypersonic Wind Tunnel of the NASA Ames Research Center in a cooperative experimental program involving NASA Ames and McDonnell Douglas Corporation. The model design and test planning were performed in close cooperation with members of the Ames computational fluid dynamics team for the National Aero-Space Plane program. Experimental results are presented, consisting primarily of flowfield surveys with five-hole and thermocouple probes. The probe data consist of impact-pressure, flow-direction, and stagnation-temperature profiles in the interaction flowfield. The impact-pressure distributions are complex, as a result of multiple shock waves and the large differences in both reservoir pressure and temperature between the jet and the external flow. The thermocouple-probe surveys give a clear indication of the shear layer between the jet and the external flow. Cross-section views of shock-wave and shear-layer locations constructed from the probe data show that the flow is highly three-dimensional throughout the region of investigation.

Nomenclature

T = temperature
u = velocity
α = angle of attack
β = yaw-plane flow inclination angle, positive to right when facing in positive x direction
σ = local pitch-plane flow angle measured in jet-plume x–z coordinate system (zero is parallel to the x axis; positive is downward deflection)

Subscripts

s = thermocouple-probe support temperature
0 = thermocouple-probe corrected junction temperature
2 = conditions downstream of a normal shock wave

Introduction

THIS paper is the second in a two-part series presenting results of an experiment on the flowfield created by the interaction of a single-expansion-ramp nozzle (SERN) with an external hypersonic flow. The first part[1] presents a discussion of the generic model concept and test procedures, oil-flow and shadowgraph flow-visualization data, boundary-layer rake data, and Preston-tube data. This paper is devoted primarily to presentation of five-hole and thermocouple-probe surveys in the jet plume and the surrounding external flow. This investigation is part of a cooperative program between McDonnell Douglas Corporation (MDC) and the NASA Ames Research Center, and was supported in part by the McDonnell Douglas Independent Research and Development Program.

Experimental Methods

Model and Traversing Mechanism

The experiment was conducted in the NASA Ames 3.5-Ft Hypersonic Wind Tunnel. The primary features of the SERN model are described in Ref. 1. Figure 1 shows a schematic of the model and traversing unit installed in the tunnel test section. The traversing unit mounts above the model. A holder for five-hole and thermocouple probes used for flowfield surveys is mounted on a horizontal tube, which is attached to a strut, the lower part of which is immersed in the tunnel flow. The upper part of the strut attaches to a positioning table that is remotely driven vertically by a motor–encoder assembly. The vertical positioning table is mounted in turn on a horizontal positioning table that is remotely driven in the cross-stream (y) direction. The mechanism is assembled inside of a rigid box structure; the horizontal positioning table is bolted to members that form the lower side edges of the box. Streamwise movement is accomplished by unbolting and reattaching the positioning-table assembly between runs.

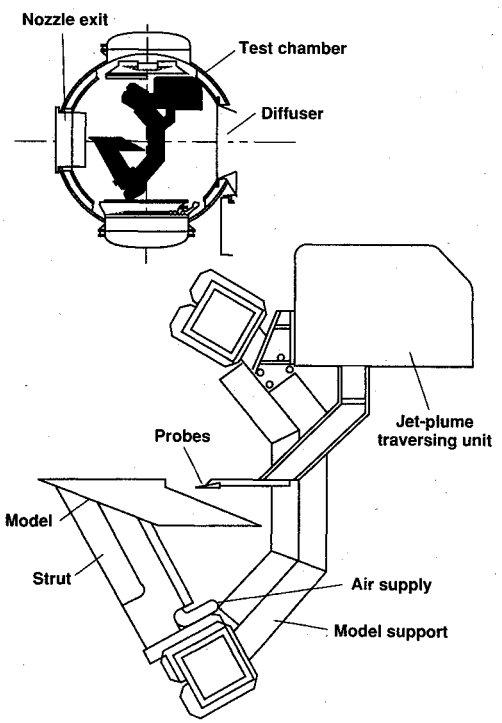

Fig. 1 Schematic of model and jet-plume traversing unit installed in test section of NASA Ames 3.5-Ft Hypersonic Wind Tunnel.

Received April 22, 1994; revision received July 6, 1995; accepted for publication July 6, 1995.

*Group Manager, Experimental Fluid Dynamics, Advanced Flight Technology. Associate Fellow AIAA.
†Research Scientist, NASA Ames Research Center, MS 203-2, Moffett Field, CA 94035-1000. Associate Fellow AIAA.

The two arms of the model-insertion mechanism are shown connected by a C-shaped structure (C strut). The model-support strut is attached to the lower arm of the insertion mechanism, and the traversing unit is attached to the C strut near the upper arm. Prior to a run, the entire apparatus is retracted from the freejet test section. After the flow is established, the model is inserted, and prior to tunnel shutdown it is retracted. Although the structure containing the positioning tables and motor–encoder assemblies is located above the test-section jet during a run, this assembly is exposed to significant transient heating from the recirculating test-cabin flow.

Probe Configurations and Data-Reduction Procedures

Sketches and photographs of the five-hole and thermocouple probes used with the jet-plume traversing unit are shown in Fig. 2. The five-hole probe is a type commonly used to measure total pressure and flow direction. The large size chosen for this probe resulted from requirements for robustness and small probe-pressure lag time.

The design, calibration, and data reduction for the five-hole probe followed the method outlined by Dudzinski and Krause.[2] Calibrations were performed in the 3.5-Ft Hypersonic Wind Tunnel at the baseline test conditions, and in a freejet calibration facility at MDC at Mach numbers of 2.5 and 3.5. Calibration data at the lower Mach numbers were obtained in a Reynolds-number range representative of flow within the jet plume. The effect of Mach number on the calibration data was found to be small and was neglected. The five-hole-probe data were reviewed to determine the applicability of the calibration data. Use of the calibration data requires that spatial variations in local flowfield properties be small relative to the probe height or width. This criterion is violated within the ramp boundary layer and at shock waves. At such locations, the impact pressure was assumed to be the maximum value measured by any of the probe ports, and the values of σ and β were discarded. A small number of total-pressure data points in any one survey include data reduced in this manner. The uncertainty of data reduced in this approximate manner is estimated to be ±3%.

The thermocouple probe is a type described by Kussoy et al.[3] and is sketched in Fig. 2b. The chromel–alumel probe is a three-support unit with two junctions, as shown. The sensor junction is located at the center of the horizontal wire, and the other junction is located at the tip of one support. Conduction and radiation corrections were applied to the data obtained with the thermocouple probes, following the procedure described by Vas[4] and using a data-reduction program supplied by Horstman.[5] The conduction correction is a function of the Reynolds number based on the probe wire diameter and local flow conditions at the wire. The value of this Reynolds number remained above approximately 200 for the flow conditions of this experiment. In this Reynolds-number range, the conduction correction function is not sensitive to variations in Reynolds number, so that only a crude estimate of the Reynolds number is needed.

During a survey, the probe tips were positioned at the same x and z locations, but the thermocouple probe was positioned in the probe holder 3.2 cm outboard of the five-hole probe.

Test-section freestream conditions, jet-stagnation conditions, jet mass-flow rate, and model static-pressure data were acquired by the NASA data-acquisition computer. These data were transferred to both a NASA minicomputer and an MDC minicomputer for analysis. The traversing unit was controlled and the probe pressure and position data were acquired by the MDC minicomputer.

Test Conditions and Accuracy

The baseline test conditions established for this experiment are presented in detail in Ref. 1, including nominal values, variations among runs, and variations within runs. Pertinent nominal values are as follows: $M_\infty = 7.33$, $Re/m = 14.0 \times 10^6$, $p_{tj}/p_\infty = 310$. The estimated probable uncertainties of pertinent recorded and calculated quantities are as follows: M_∞, $T_{t\infty}$, T_{tj}, and $p_{t\infty}$, ±2%; Re/m, ±8%; σ, ±2 deg; β, ±3 deg; probe p_{t2}, ±1%; model static pressures, ±0.09 kPa; thermocouple probe temperature, ±2% at $T_{t\infty}$, ±1% at T_{tj}; probe location resolution, ±0.15 cm; and position uncertainty, ±0.25 cm.

Results and Discussion

Shadowgraph Flow Visualization

Figure 3 is a shadowgraph of the aft part of the model, which shows the interaction of the underexpanded jet plume with the external flow. Features associated with the plume include the shear layer between the jet and the external flow, the shock within the plume, and the shock in the external flow resulting from the expansion of the jet flow. The turbulent boundary layer on the forebody thickens on the cowl and separates slightly forward of the cowl trailing edge because of the compression corner produced by the jet and the cowl curvature. The shock wave from the model leading edge and the disturbance from the boundary-layer trip can be seen emanating from the left side of the photograph. Streamwise locations of the four probe survey stations are indicated by the vertical lines; z locations of the spanwise traverses are also shown.

Ramp Static-Pressure Distributions

Ramp static-pressure distributions are presented in Fig. 4. Figure 4a shows the ramp surface pressure distribution corresponding to the baseline test conditions. The centerline row, starting at the internal nozzle combustor station, is the most complete. The character of the centerline distribution is similar to that of previous

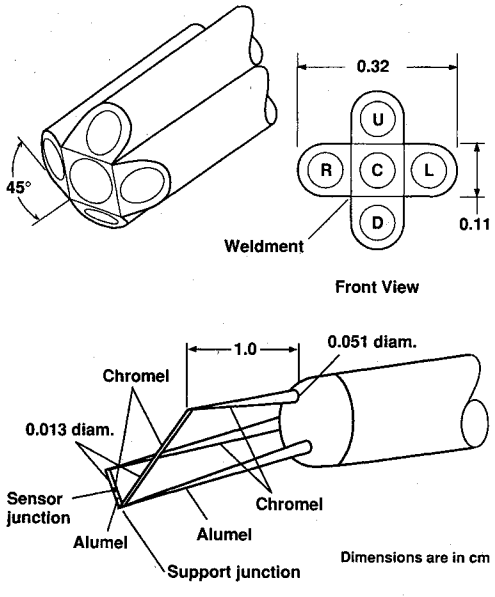

Fig. 2 Sketches of jet-plume traversing-unit probes: a) five-hole probe tip and b) thermocouple probe.

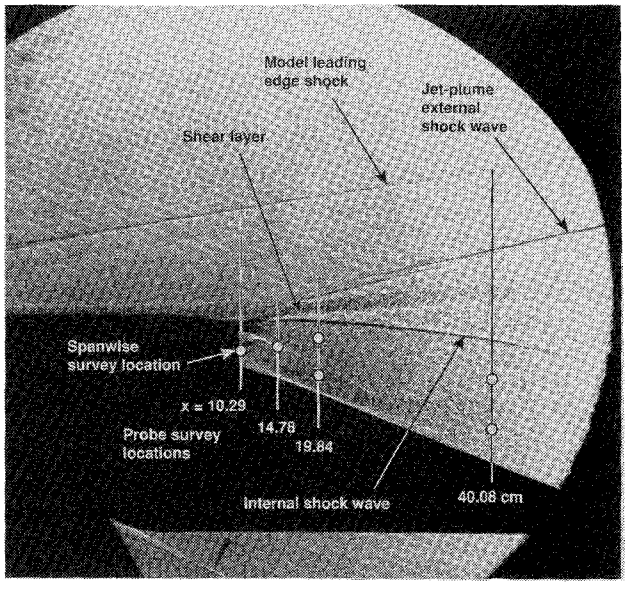

Fig. 3 Shadowgraph photograph at baseline test condition, showing features and locations of vertical and transverse surveys.

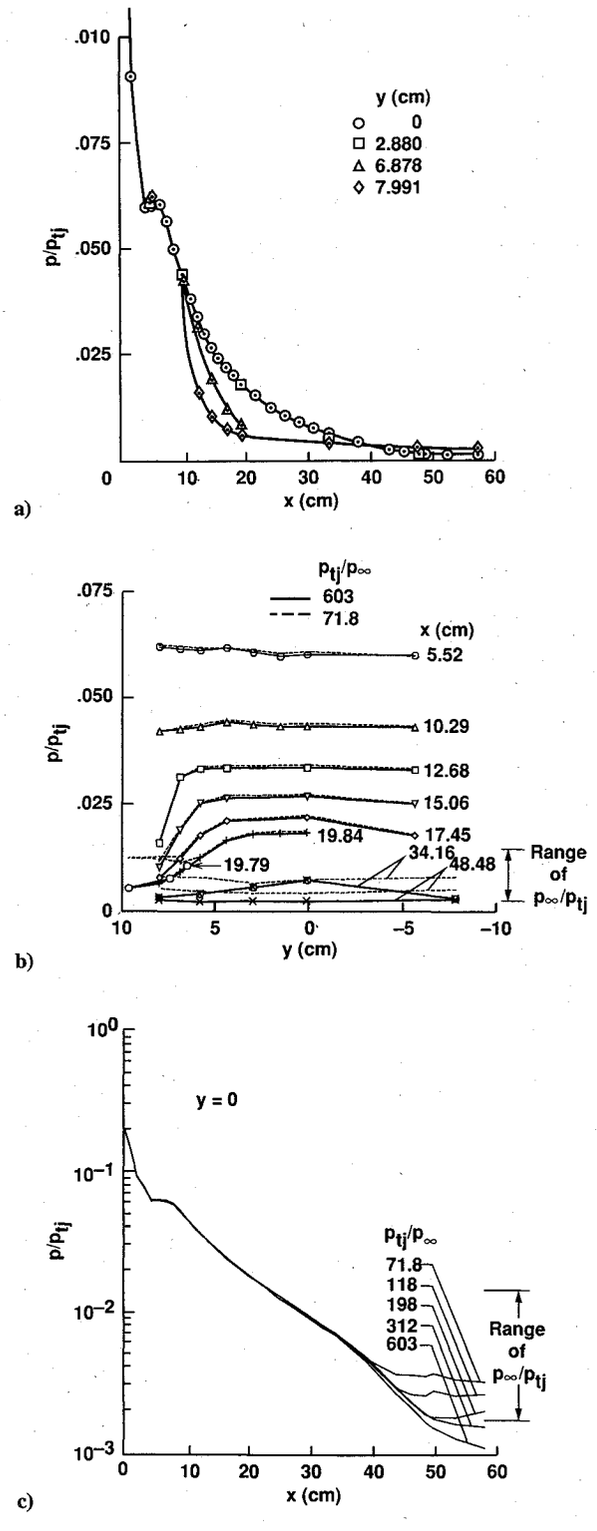

Fig. 4 Ramp static-pressure distributions: a) streamwise distributions at various values of y, baseline conditions, b) transverse distributions at the maximum and minimum pressure ratios, and c) streamwise centerline distributions for various pressure ratios.

nozzle studies. The outboard pressure distributions show that the pressures decrease toward the model side edge because of the outward expanding flow. The pressures are equal on each side, thus indicating symmetrical flow.

A series of transverse ramp static-pressure distributions are presented in Fig. 4b. Data from two runs are superimposed, corresponding to $p_{tj}/p_\infty = 71.8$ and 603, the limits of the range of pressure ratios explored in this study. The range represented by p_∞ in these coordinates is also shown. Note that the pressure distribution on most of the ramp is unaffected by variations in p_{tj}/p_∞. At the larger values of x, an influence of pressure ratio appears on the sides, and apparently just reaches the centerline at $x = 34.16$ cm. Only at the row of pressure orifices located furthest downstream, $x = 48.48$ cm, is the influence of variation in pressure present for all values of y.

The linear ordinates used in the preceding two plots deemphasize pressure variations at the downstream end of the ramp. Figure 4c presents a comparison of data on the ramp centerline for the full range of pressure ratios using a logarithmic scale for the ordinate. Individual data points are omitted for clarity. The range represented by p_∞/p_{tj} is also shown. This comparison shows that the centerline pressure distribution is independent of pressure ratio for $x < 40$ cm. Further downstream, the centerline pressure distribution is a function of pressure ratio, but the ramp pressure always expands below p_∞.

Five-Hole- and Thermocouple-Probe Data

Figure 5 consists of two composite views of the jet-plume–external-flow interaction along the model centerline obtained from five-hole- and thermocouple-probe data at the baseline test conditions ($p_{tj}/p_\infty = 310$). The data of Fig. 5a were obtained along the model centerline (the x–z plane, side view), and Fig. 5b shows data from four spanwise traverses (top view).

Features of the model geometry shown here include the cowl external contour, the jet flow passage beginning at the combustor exit station, and the ramp surface. Probe data are shown for the four axial stations surveyed in this experiment. The solid lines represent distributions of the impact pressure p_{t2}: the local pitot pressure downstream of a normal shock corrected for the effect of misalignment between the probe axis and the local velocity vector. The thermocouple-probe data (dashed lines) are presented as the excess of the local total temperature above the value in the jet normalized by the overall temperature difference, $(T - T_{tj})/(T_{t\infty} - T_{tj})$. Scales for these quantities are given. Individual data points have been omitted for clarity; examples of surveys showing individual data points are shown later.

The p_{t2} survey obtained at $x = 10.29$ cm shows the outer portion of the ramp boundary layer, the variation within the jet resulting from the variation in local Mach number, the impact-pressure defect associated with the separated forebody boundary layer, and variations presumably associated with disturbances from the boundary-layer trips and the leading-edge shock wave. No total-temperature data were obtained at this station.

Both impact-pressure and total temperature distributions are presented at the three downstream stations, $x = 14.78$, 19.84, and 40.08 cm. (The limited extent of the data corresponding to $x = 14.78$ cm is the result of a premature tunnel shutdown.) The value of obtaining both pressure- and temperature-probe data is illustrated by this figure, since it emphasizes the degree to which the two types of probes respond to different flowfield features. Discontinuities in p_{t2} caused by the shock wave within the plume and the external shock wave are evident in the profiles obtained at the three downstream stations (see arrows). The locations and thicknesses of the shear layer between the jet and the external flow are shown by the total-temperature distributions. A comparison of the impact-pressure and total-temperature data shows that the aspects of the shear layer originating with 1) the forebody boundary layer and its separation and 2) the interaction between the jet and the external flow are independently identifiable, even at $x = 40.08$ cm. Evidence of the forebody boundary layer is given by the relatively thick layer of total-pressure defect at the cowl exit, which is seen to persist in the downstream profiles. The shock waves and the shear layer indicated by the total temperature survey are initially embedded within this layer of total-pressure defect.

The character of the impact-pressure distribution is similar at the three downstream stations, showing a local minimum between the shocks in each case. These results suggest a degree of similarity of the impact-pressure distributions if the separation between the shocks is used as a length scale and the local maximum impact-pressure difference is used to scale the impact-pressure data. Note that there are no indications of shock waves in the total-temperature distributions, as expected, even though the local flow properties and

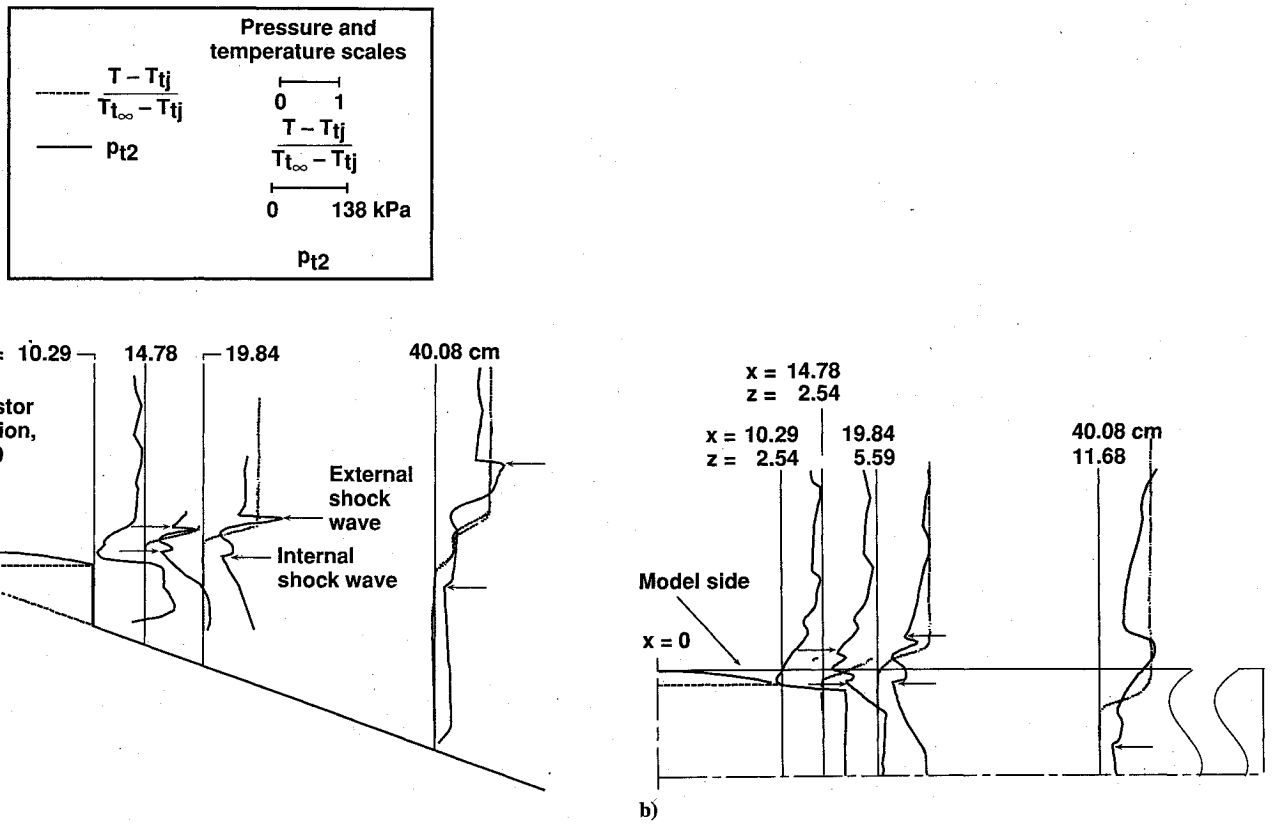

Fig. 5 Composite views of impact-pressure and total-temperature distributions, baseline test conditions, $p_{tj}/p_\infty = 310$: a) surveys in symmetry plane, $y = 0$ and b) spanwise surveys, $2.5 < z < 11.7$.

the associated conduction corrections change significantly as the shocks are traversed.

At $x = 14.78$ and 19.84 cm, the minimum in the distribution of p_{t2} corresponds approximately with the center of the shear layer as indicated by the total-temperature distribution. At $x = 40.08$ cm, however, this feature of the impact-pressure distribution corresponds more nearly to the outer edge of the shear layer as indicated by the temperature profile. At this streamwise station, two sets of temperature-profile data are presented. These data are identical, except for an apparent y-position offset, and show two distinct layers with an intermediate region of approximately constant total temperature. This type of temperature distribution is different from that obtained at the two upstream stations, and also different from all of the temperature distributions obtained from cross-stream (z = constant) surveys, to be presented later. The cause of this unusual temperature distribution in the x–z plane at $x = 40.08$ cm is not known.

Figure 5b gives the corresponding plan view of the flowfield. These traverses do not lie in the same plane, but were obtained at roughly comparable distances from the ramp surface; the data for $x = 19.84$ and 40.08 cm correspond to the larger of the two z values for which data were obtained at these streamwise stations.

Many features of Fig. 5a are also present in Fig. 5b: the boundary layer separated from the external surface of the cowl, the internal and external shock waves, and the proximity of the shear-layer location indicated by the total-temperature profile to the minima in the impact-pressure distributions. In the plan view, the jet impact-pressure profile is uniform at $x = 10.29$ cm. Profiles of p_{t2} at the next two stations downstream clearly show the progress of the cowl trailing-edge expansion. Both the spanwise pressure and temperature profiles for $x = 40.08$ cm are significantly different from their counterparts in Fig. 5a. The spanwise temperature profile does not show a two-layer structure. The internal shock wave is near the model centerline in the spanwise pressure profile, and the external shock wave does not appear as a sharp discontinuity.

Figure 6 presents detailed survey data at $x = 19.84$ cm and $z = 5.58$ cm. Profiles of p_{t2}, σ, β, and T_t are presented. Two runs

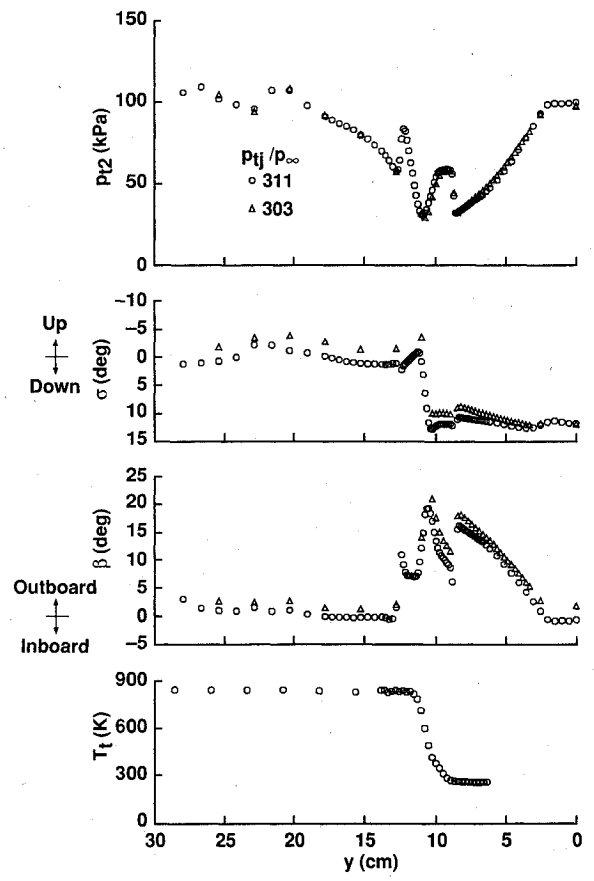

Fig. 6 Impact pressure, flow angle, and total-temperature data at $x = 19.84$ cm, $z = 5.58$ cm.

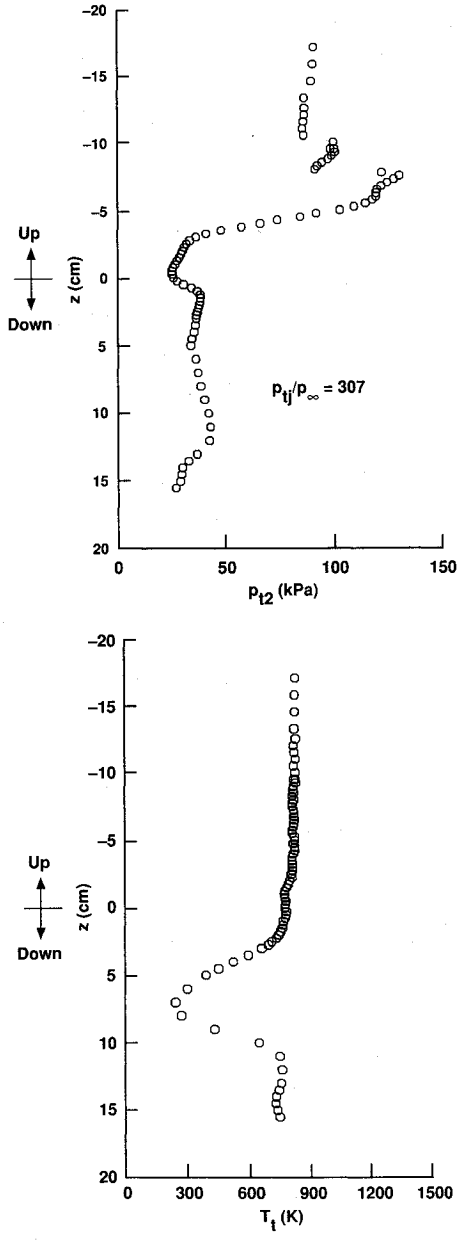

Fig. 7 Impact pressure and total temperature data at x = 40.08 cm, impact pressure at y = 6.35 cm, and total temperature at y = 9.55 cm.

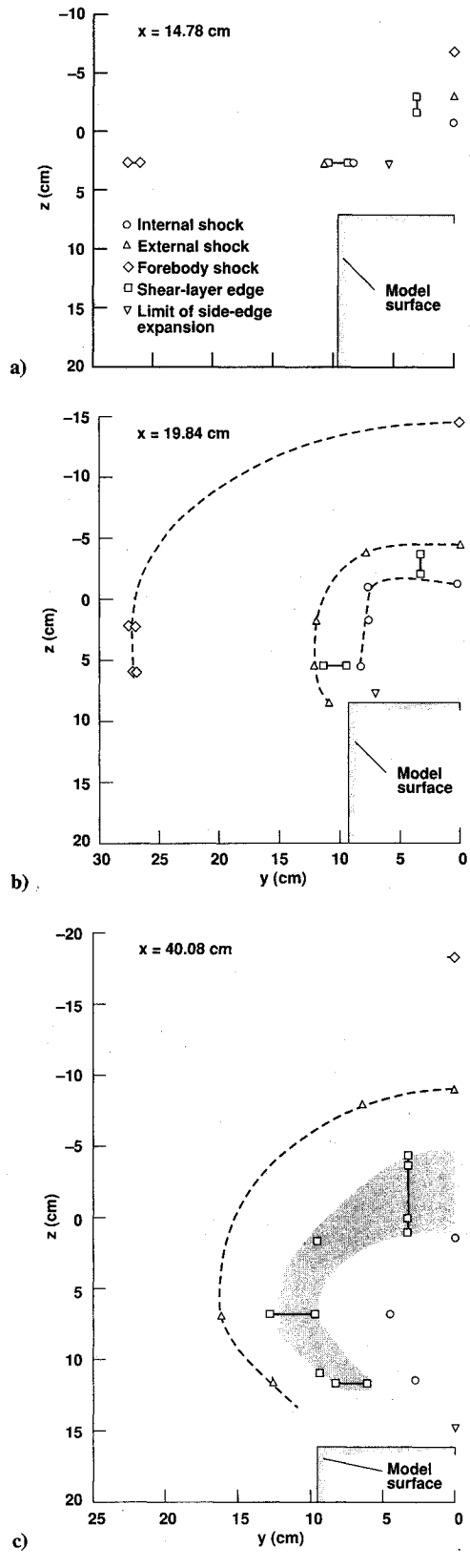

Fig. 8 Shock-wave and shear-layer locations obtained from probe data, baseline test conditions.

with the five-hole probe and a total-temperature survey are included. The good repeatability of the p_{t2} distribution and the slightly poorer repeatability of the σ and β distributions arise from the fact that impact pressure involves a small correction to a primary measured quantity, but the flow-direction angle depends on the difference between two measurements of similar magnitude. The data show a central region of the jet with constant properties and the influence of the cowl side-edge expansion resulting in decreasing p_{t2} and increasing outboard flow direction with increasing y. The internal shock, shear layer, and external shock are most evident in the p_{t2} and β distributions. The pitch-plane flow inclination angle outboard of the external shock is small. The flow within the jet shows a significant downward velocity component resulting from proximity to the ramp. The total-temperature distribution shows constant levels with a monotonic variation between. The shear layer, indicated by the total-temperature distribution, also coincides approximately with the local minimum in the impact-pressure distribution.

Results of five-hole- and thermocouple-probe surveys at x = 40.08 cm are presented in Fig. 7. The spanwise locations of the five-hole-probe survey and the thermocouple-probe survey are 6.35 and 9.55 cm, respectively. The impact-pressure distribution shows lower values and less linear variation than the distribution obtained at $y = 0$. For $z < 0$, the difference between the $y = 0$ profile and the outboard profile is substantial. The latter profile shows no clear evidence of the internal shock in the p_{t2} profile. The p_{t2} distribution in the shear layer is qualitatively different from the centerline profile, exhibiting a broad minimum where the centerline data show a maximum. There is also evidence of two external shocks in the p_{t2} distribution.

Because the total-temperature probe is outboard of the five-hole probe, the total-temperature profile of Fig. 7 is only 0.13 cm inboard of the side of the model. A significant finding of this total-temperature survey is the fact that the jet flow does not cover the ramp at this streamwise station; flow from the external stream present above the ramp. Two outer shear-layer edges are present in this profile, and the minimum temperature is only slightly greater than the jet total temperature, indicating that this profile is approximately tangent to the inner edge of the shear layer.

Sketches of the Jet–External-Flow Interaction

Shock-wave and shear-layer locations obtained from the probe data are shown in cross-section views, in Fig. 8, for the three downstream survey locations. Few surveys were obtained at $x = 14.78$ cm, and the data are insufficient to allow sketching the intermediate locations of features with reasonable confidence. More data were obtained at $x = 19.84$ and 40.08 cm, however, and shock-wave and shear-layer locations have been sketched to aid interpretation of the data. Estimates of ramp boundary-layer thicknesses obtained from the rake data are also included at these downstream stations. The shear layer as indicated by the temperature-probe data nearly fills the region between the internal and external plume shocks at the two upstream stations, but these features become more widely separated at $x = 40.08$ cm. The shape of the internal shock wave changes significantly between the two downstream stations, and the shear layer is clearly seen to approach the ramp inboard of the ramp side edge in Fig. 8c. At the two upstream stations, the shear layers are seen to be significantly thicker at the sides than at the centerline, but the trend is reversed at the downstream station. The flow at $x = 40.08$ cm is highly three dimensional.

Concluding Remarks

Data were obtained from an experiment conducted with a generic nozzle–afterbody model in the 3.5-Ft Hypersonic Wind Tunnel of NASA Ames Research Center to characterize experimentally the flowfield created by the interaction of a SERN flow with a hypersonic external stream. This paper presents experimental results consisting of five-hole- and thermocouple-probe surveys, with examples of static-pressure distributions and a shadowgraph photograph.

The static-pressure distribution normalized by the jet total pressure is independent of jet-to-freestream pressure ratio for a major portion of the ramp surface. Probe surveys were conducted at four streamwise stations. The impact-pressure distributions are complex, as a result of multiple shock waves and the large differences in both reservoir pressure and temperature between the jet and the external flow. The thermocouple-probe surveys give a clear indication of the shear layer between the jet and the external flow. A comparison of the impact-pressure and total-temperature data shows that aspects of the shear layer originating with the forebody boundary layer and the interaction with the jet and the external flow are independently identifiable for a considerable distance downstream of the cowl exit location. Cross-section views of shock-wave and shear-layer locations constructed from the probe data show that the flow is highly three-dimensional throughout the region of investigation. Shear-layer thicknesses obtained from thermocouple-probe surveys show significant differences between vertical and spanwise traverses.

Acknowledgments

This research was conducted by the NASA Ames Research Center in cooperation with the McDonnell Douglas Independent Research and Development Program.

References

[1]Keener, E. R., and Spaid, F. W., "Hypersonic Nozzle–Afterbody Experiment: Flow Visualization and Boundary-Layer Measurements," *Journal of Spacecraft and Rockets*, Vol. 33, No. 3, 1996, pp. 326–332.

[2]Dudzinski, T. J., and Krause, L. N., "Flow Direction Measurements with Fixed-Position Probes," NASA TM X-1904, 1969.

[3]Kussoy, M. I., Horstman, C. C., and Acharya, M., "An Experimental Documentation of Pressure Gradient and Reynolds Number Effects on Compressible Turbulent Boundary Layers," NASA TM 78488, June 1978.

[4]Vas, I. E., "Flowfield Measurements Using a Total Temperature Probe at Hypersonic Speeds," *AIAA Journal*, Vol. 10, No. 3, 1972, pp. 317–323.

[5]Horstman, C. C., private communication, NASA Ames Research Center, Moffett Field, CA, Sept. 1990.

K. J. Weilmuenster
Associate Editor